



Published in final edited form as:

IEEE Trans Biomed Eng. 2011 June ; 58(6): 1874–1880. doi:10.1109/TBME.2011.2131141.

Indices and Detectors for Fetal MCG Actography

William J. Lutter and Ronald T. Wakai

Department of Medical Physics, University of Wisconsin, Madison, WI 53706 USA

William J. Lutter: wjlutter@wisc.edu; Ronald T. Wakai: rtwakai@wisc.edu

Abstract

Several recent studies have demonstrated the usefulness of fetal magnetocardiogram (fMCG) actography, a relatively new method of detecting fetal movement that can be performed in conjunction with fMCG assessment of fetal heart rate and rhythm. In this work, we formulate indices of fetal activity that incorporate information from all channels to achieve improved sensitivity. We also utilize statistical detection to provide an objective means of inferring significant fetal activity.

Index Terms

fetal actography; fetal magnetocardiography; fetal movement

I. Introduction

Recently, fetal magnetocardiography (fMCG) has received considerable attention as a highly effective means of diagnosing fetal rhythm abnormalities. In addition to assessing fetal heart rate and rhythm, an important, but lesser known, capability of fMCG is detection of fetal activity. fMCG actography was first described by Zhao and Wakai in 2002 [1]. In that study and in others [2] fMCG actography was used to assess fetal reactivity, which refers to the association between fetal heart rate acceleration and fetal movement seen in healthy fetuses during the last trimester. Evaluation of fetal reactivity is the basis of non-stress testing and is the primary obstetrical application of fetal actography. Interestingly, however, fMCG actography has been effectively utilized in several other diverse situations. In a study of fetuses with supraventricular tachycardia, an arrhythmia characterized by abrupt onset and cessation, Wakai and coworkers used fMCG actography to demonstrate that the rhythm changes usually coincided with episodes of fetal activity [3]. In a study of several normal fetuses, Popescu and co-workers used fMCG actography to show that unusual signals they attributed to fetal hiccups could not be due to gross fetal movement [4]. Lastly, in a study of fetal brain activity, McCubbin and co-workers used fMCG actography to aid in artifact rejection, which provided a significant increase in the signal-to-noise ratio (SNR) of fetal visual evoked responses [5].

fMCG actography is based on detection of changes of fetal QRS amplitude arising from changes in position and orientation of the fetal heart due to fetal movement. Fetal movement alters other aspects of the fMCG tracing, such as the signal baseline and the QRS configuration, but signal baseline changes are often caused by artifact unrelated to fetal activity and QRS configuration changes are more complicated to assess than QRS amplitude changes. Moreover, QRS amplitude is readily obtained in the course of QRS detection for

fetal heart rate computation, and the point-by-point correspondence of the actogram and heart rate tracings facilitates the plotting of the actocardiogram.

The methodology used by Zhao and Wakai [1] was very simple. They constructed tracings of the instantaneous amplitude of the fetal QRS complex, and inferred fetal trunk movement from amplitude changes. Although the recordings were made with a multi-channel magnetometer, only information from the channel with the largest QRS amplitude was used. For a multi-channel magnetometer, fetal movement generally alters the signal amplitude of each channel, corresponding to a change in the signal topography, i.e. spatial pattern. In this report, we improve upon previous efforts by evaluating several new indices of fetal activity that incorporate information from all channels. In addition, detectors are implemented to provide an objective means of inferring significant activity.

II. Methods

A. Candidate Movement Indices

Perhaps the most direct way of inferring movement is to track the source location by applying a source localization technique, such as dipole fitting; however, this is not always possible because accurate dipole fitting requires a high SNR and adequate coverage of the signal topography. The latter may be compromised by poor detector placement or by large fetal movement. A simple alternative to source localization is to track shifts of the signal topography. This was accomplished here by computing the “center-of-mass” of the signal topography in the plane of the sensor array by weighting the channel position by the square of the signal amplitude. Neglecting the modest curvature of our sensor array and assuming that the central channel lies at the origin with its normal pointing in the z direction, the x and y coordinates of the signal center-of-mass, x_{CM} and y_{CM} , respectively, were computed as a function of time. An alternative approach that turns out to be highly effective is to track changes in signal space. At each instant of time, the output of our 37-channel sensor is described by a 37-component signal space vector, \mathbf{X} . For each heartbeat, we tracked the magnitude (L2 norm) of \mathbf{X} , $r_{SS}=|\mathbf{X}|$, and the signal space angle, $\theta_{SS}=\cos^{-1}(\mathbf{X}\cdot\mathbf{X}_0/|\mathbf{X}||\mathbf{X}_0|)$, where \mathbf{X}_0 is the initial \mathbf{X} . While r_{SS} is a measure of the overall signal strength across the array, θ_{SS} denotes the spatial pattern. In addition, a signal space “velocity”, $v_{SS}=|\Delta\mathbf{X}/\Delta t|$, was computed from the magnitude of the beat-to-beat change, divided by the RR interval. Unlike the other indices, v_{SS} depends directly on the RR interval, which accentuates variations of v_{SS} that occur during heart rate accelerations.

The signal-space velocity, v_{SS} , which is computed from the beat-to-beat amplitude changes, rather than from the amplitudes, offers several advantages. First, it has zero mean since it derived from the time difference, whereas the other indices may have a large mean. Second, it condenses the information into a single index, whereas r_{SS} and θ_{SS} provide additional information at the cost of assessing two paired indices. Last, and most important, the components of $\Delta\mathbf{X}/\Delta t$ are approximately central Gaussian, which allows the use of standard detectors, whereas the components of \mathbf{X} , on which the other indices are based, generally do not exhibit a Gaussian distribution. Gaussianity can be assessed using the Lilliefors test. If the fetus jitters about a single position and orientation due to incidental body movement, as seen commonly during fetal heart rate (FHR) pattern A [6], then the components of \mathbf{X} may be approximately Gaussian; however, if it shifts to a different position and remains there for an extended period then they will not be Gaussian.

B. Simulations

Simulations were performed to examine the sensitivity of the movement indices to various types of simulated movements. The fMCG source was modeled using a current dipole in a

homogeneous conducting sphere. The mean position of the dipole was 8 cm below the sphere surface, but the position was varied systematically to simulate changes in source depth, lateral position, and orientation, varying only one parameter at a time. The dipole strength was 200 nA-m, corresponding to a typical value [7], and the white noise per channel was 10^{-14} T/(Hz)^{1/2} in a 100 Hz bandwidth, corresponding to the approximate noise of our sensor. The sphere radius was assumed to be 50 cm to approximate the small curvature of the maternal abdomen. The sensor array was modeled after our 37-channel Magnes biomagnetometer (4D Neuroimaging, San Diego), with the channels distributed uniformly over a circular area of radius 13.7 cm. The center channel of the array was located on the z-axis on the sphere surface with its normal pointing in the z direction. A potential source of confusion is that the source location is specified in sphere coordinates, whereas the indices x_{CM} and y_{CM} are computed with respect to the sensor coordinates. For these simulations, however, the two coordinate systems are aligned, except for a 50 cm displacement in the z-direction.

C. MCG Recordings

The fMCG recordings used in the analysis were selected retrospectively from a database of more than 100 uncomplicated pregnancies. The data presented below were taken from the 10 most recent subjects. Gestational age at the time of study was 21–39 weeks, with mean gestational age 30.0 weeks. The recordings were made in a magnetically-shielded room, using a 37-channel biomagnetometer (Magnes, 4D Neuroimaging). Several runs of duration 10 minutes were recorded from each subject; only runs without periods of signal dropout were used. The passband was 0.1–200 Hz, and the sampling rate was 520 Hz. A digital filter was applied to further band-limit the signals to 1.0–80 Hz. The maternal MCG was removed using a matched filter. Autocorrelation was used to perform QRS detection and the amplitudes of QRS complexes in each channel were measured. A 0.2 Hz low-pass filter was used to smooth the amplitudes prior to computing the indices.

In addition to fetal recordings, we also obtained MCG signals from a neonatal subject at age 4 weeks. The signals were actually taken from a neonatal MEG recording; i.e. the detector was positioned over the baby's head. This resulted in MCG signals of amplitude ≤ 1 pT in the channels in the lower half of the sensor array, closest to the baby's heart. The main benefit of using neonatal data is that the baby's movement could be visually monitored. In addition, there was no maternal interference or confounding maternal movement.

D. Movement Detectors

We investigated two methods of detecting movement: a chi-square detector and a General Gaussian Detector (GGD). These were applied to the components of $\Delta\mathbf{X}/\Delta t$. During fetal quiescence, the components were assumed to be Gaussian with zero mean. We verified that during fetal heart rate (FHR) pattern A [6], corresponding to fetal quiescence, the majority of the components are Gaussian based on the Lilliefors test, whereas during FHR pattern B, corresponding fetal activity, the majority are non-Gaussian (Table 1).

In practice, the rank of $\Delta\mathbf{X}/\Delta t$ is low compared to the rank of the data, and the detection sensitivity is increased by eliminating components that are dominated by noise. We therefore used singular value decomposition (SVD) to rank-reduce $\Delta\mathbf{X}/\Delta t$, retaining enough SVD components to account for 90% of the power. Following rank-reduction and whitening, v_{SS}^2 was assumed to follow a Chi-squared distribution with degrees of freedom equal to the data rank. Applying a right tail probability test, we identified outliers, which were presumed to result from fetal movement, using a user-specified right tail probability $p < 0.05$.

We also implemented a GGD following the formulation of Kay [8]. The GGD assumes that the components of $\Delta\mathbf{X}/\Delta t$ are comprised of a superposition of Gaussian signal and Gaussian noise with different variances. The noise is assumed to arise from detector noise and from incidental body movements during fetal quiescence, and forms the main body of the distribution. The signal is assumed to have much higher variance, and dominates the tails of the distribution. The signal and noise statistics are estimated using freeware Matlab routines that implement the Expectation Maximization algorithm to construct maximum likelihood estimates of the parameters of a 2-component Gaussian mixture model. The detector threshold value is computed based on a user-specified probability of false positives (P_{FP}).

III. Results

A. Simulation results

The simulation results in Fig. 1 allow us to understand how the candidate indices vary for different types of movement. Ideally, the indices should have high sensitivity to all types of movement so that movement-related changes can be resolved above the background fluctuations due to noise. The sensitivity of an index to a particular type of movement is given by the derivative of the index with respect to the appropriate source parameter; i.e. position coordinate or orientation angle. It can be seen in Fig. 1 that the sensitivity varies substantially for the different types of movement and is a function of position and orientation. Fluctuations in the indices due to sensor noise manifest as jitter in the graphs.

The indices x_{CM} and y_{CM} accurately reflect lateral movement of the source in some circumstances, as exemplified in Fig. 1 by x_{CM} ; however, the accuracy is confounded by the limited coverage area of the sensor, which can result in paradoxical movement, as exemplified by y_{CM} , which shows a negative slope in the middle section of the graph despite translation in the positive direction. This occurs because the computed center-of-mass shifts opposite to the true movement as high-amplitude regions of the signal topography move beyond the range of the sensor. Another type of paradoxical movement can be seen for θ_{SS} , x_{CM} , and y_{CM} during nutation, corresponding to the lower three graphs on the far right of Fig. 1. As discussed below, these indices are insensitive to nutation and should be constant; however, as the nutation angle approaches 90° the dipole becomes purely radial, causing the signal amplitude to vanish. The mean of each index approaches a value corresponding to that of a purely random signal dominated by noise.

A common metric of performance is resolution, which is equal to the root-mean-square (rms) fluctuation divided by the sensitivity; however, the resolution is difficult to plot for our data because it becomes infinite when the sensitivity is zero, corresponding to regions with zero slope in Fig. 1. Instead we plot in Fig. 2 the reciprocal of the resolution—absolute value of the derivative with respect a given source parameter divided by the rms fluctuation—which we call the normalized sensitivity, S_Φ , where Φ is one of the movement indices (amplitude of the channel with largest signal, x_{CM} , y_{CM} , r_{SS} , θ_{SS}), x is one of the source parameters (lateral position, depth, precession angle, nutation angle), and $\langle\Phi^2\rangle^{1/2}$ is the rms noise.

$$S_\Phi(x) = |\partial\Phi/\partial x|/\langle\Phi^2\rangle^{1/2} \quad [1]$$

The normalized sensitivities show complicated behavior, but insight can be gained by considering how the different types of movement alter signal amplitude and topography. Dipole precession and lateral translation produce marked changes in spatial pattern, but small changes in overall signal amplitude; i.e. dipole precession and lateral translation, respectively, produce a corresponding rotation and translation of the signal topography, but

the overall signal strength (L2 norm) is largely unchanged because the source depth and the magnitude of the tangential component of the dipole, which are the two main determinants of overall signal strength, remain nearly constant. In contrast, dipole nutation and changes in source depth produce large changes in signal amplitude and small changes in spatial pattern; i.e. dipole nutation and changes in source depth, respectively, alter the magnitude of the tangential component of the dipole and the depth of the dipole, but the signal topography is largely unchanged because the lateral position of the dipole and the orientation of its tangential component remain constant. With this in mind, we observe that θ_{SS} , x_{CM} , and y_{CM} , which are formulated to track changes in signal topography, indeed show good sensitivity to dipole precession and lateral translation but poor sensitivity to dipole nutation and depth changes.

The actogram index used in previous fMCG studies is the signal amplitude of the channel with largest signal, depicted in the first row of Figs. 1 and 2. Although it derives from a single channel, it exhibits some sensitivity to all types of movement; however, r_{SS} also exhibits sensitivity to all types of movements and shows higher sensitivity. Actograms of the velocity index, v_{SS} (not shown), are difficult to simulate in a realistic manner since fetal movements are typically transient and jerky, but v_{SS} is a composite of the time differences of r_{SS} and θ_{SS} and thus exhibits sensitivity to all types of movement.

B. Detector thresholds

It is convenient to use the same detector threshold for all subjects, rather than having to determine a threshold for each subject. To aid in determination of a suitable threshold, we analyzed 16 ten-minute recordings taken from 10 subjects (6 subjects returned for a follow-up sessions), and we computed the percent detection of movement associated with 1) accelerations of amplitude 15 bpm lasting at least 15 seconds, 2) accelerations of amplitude 10 bpm lasting at least 10 seconds, and 3) FHR pattern A, normalized to the number of detections for $p=0.05$ and $P_{FP}=10^{-4}$, respectively, for the chi-square and the GGD, which yield a relatively high number of pattern A detections. The results are shown in Fig. 3. The threshold is chosen so that all 15 bpm accelerations are detected, while the number of pattern A detections remains relatively low. Based on these criteria, we chose $p=0.01$ and $P_{FP}=10^{-8}$, respectively, as the thresholds for the chi-square detector and the GGD.

Several comments are in order. First, the detectors are very sensitive and it is possible to detect all of the 15 bpm accelerations using small values of p and P_{FP} ($\ll 0.05$). In addition, the recordings that contain a mixture of pattern A and B usually give the desired results; i.e. they reliably detect movement in association with 15 bpm accelerations and rarely detect movement during pattern A. It is more difficult, however, to achieve a low number of detections in pattern A if only pattern A data are used. The pattern A results shown in Fig. 3 were obtained for this more challenging scenario, in which detection is performed using statistics derived solely from pattern A data. Second, 15 bpm FHR elevations above baseline lasting at least 15 seconds are universally considered to be accelerations that are associated with movement; however, 10 bpm FHR elevations lasting at least 10 seconds are also considered by some to be accelerations that are associated with movement. If desired, the user can adjust the threshold to increase or decrease the detection of these accelerations. Third, we do not expect the fetus to be motionless during FHR pattern A; it is likely that occasional small movements occur. Thus, the pattern A detections are not necessarily false alarms. Lastly, the detectors normalize each component of v_{SS} by the variance of the component. It is therefore possible for a smaller peak in v_{SS} to have a higher statistical significance than a larger peak.

Fig. 4 shows how the number of detections varies for the chi-square detector and the GGD for different values of p and P_{FP} , respectively, when applied to the v_{SS} actogram of a

representative normal fetus at 34.5 weeks' gestation. Notice that the GGD is more sensitive than the chi-square detector, e.g. the detections of the chi-square detector for $p=0.005$, 0.01 , and 0.05 , respectively are similar to those of the GGD for $P_{FP}=10^{-12}$, 10^{-8} , and 10^{-4} . If desired, the detectors can be made more sensitive by increasing p or P_{FP} . For example, in Fig. 4 for $P_{FP}=10^{-4}$ the GGD detects three movements during the period 250–400 s, when the FHR pattern transitions from pattern A to pattern B. These detections are associated with FHR increases that are too small to be classified as accelerations; however, it is likely that the detected movements are real, albeit less vigorous than those associated with FHR accelerations.

C. Fetal and neonatal actograms

Fig. 5 and 6 show actograms derived from each of the candidate indices. The indices show prominent changes in association with FHR acceleration, although they differ in detail, presumably because they are differentially sensitive to various types of fetal movement. Generally, we observe that the indices are highly correlated provided that the SNR is not low; i.e. when movement is detected, all of the indices show some degree of change. This suggests that real fetal movements are complex and likely involve a combination of the movements modeled in the simulations. Notice that the v_{SS} actograms are easy to interpret because they are near zero in the absence of movement. The neonatal recording (Fig. 6) allows validation via direct observation of movement. The baby was asleep during the recording, but exhibited vigorous movement lasting about 10 s in association with the two large accelerations beginning at around 370 and 520 s, similar to the reactivity seen in fetuses during FHR pattern B. The brief FHR acceleration at 425 s was associated with less vigorous movement.

IV. Discussion

This study demonstrates the advantages of using indices of fetal movement derived from all of the channels and of using statistical methods to evaluate changes in the indices. While it is possible to conceive of a multitude of indices, the signal-space indices we utilized— r_{SS} , θ_{SS} , and v_{SS} —are mathematically logical and simple. Importantly, they exhibit good overall sensitivity to fetal movement. High sensitivity is especially helpful when the signal is low amplitude. This is common at early gestational ages or can occur if the fetus moves away from the detector during the recording. The signal-space velocity, v_{SS} , exhibits additional key advantages. Its components are approximately Gaussian, which greatly facilitates the use of statistical methods. It also is simple to interpret because it is nearly zero in the absence of fetal movement, whereas the other candidate indices have a nonzero baseline. The indices x_{CM} and y_{CM} were devised to track movement of the signal topography in lieu of tracking the source position directly; however, they show poor sensitivity to some types of movement and have limited accuracy. The actograms derived from the channel with largest signal amplitude showed good overall sensitivity, attesting to the veracity of prior studies using this method, but the overall sensitivity was less than that of the signal-space indices.

Statistical methods provide an objective means of determining whether changes in the movement indices are significant at a level specified by the user. The chi-square detector is easiest to implement. It is less sensitive than the GGD, but is more conservative because it assumes that only outliers correspond to movement. The sensitivity of the GGD can be adjusted by varying P_{FP} . We found that $P_{FP}\approx 10^{-8}$ gives a good association between FHR accelerations and detected movement, but the detector can be made more sensitive, if desired, by increasing P_{FP} to allow detection of less vigorous movements.

The method described here is susceptible to interference and artifact that distorts the amplitude of the fetal QRS complexes; therefore, at a minimum, signal processing to remove maternal interference is necessary. We applied matched filtering for this purpose because it is widely used and does not reduce the rank of the data. Alternative signal processing methods can also be used. The influence of signal processing on the results is likely to depend on the specific processing method and was not investigated here.

Fetal actography is an important technique because assessment of fetal movement is a critical component of antepartum fetal surveillance. Fetuses in distress compensate by reducing their activity, resulting in fewer movements and fewer FHR accelerations. In some circumstances, however, movements occur in the absence of FHR accelerations. Prior to 27 weeks' gestation, the fetus is often active but the FHR accelerations are low amplitude. For this reason, FHR monitoring is not performed until the last trimester. The ability to correlate fetal movement with FHR accelerations of reduced amplitude could be useful for monitoring fetuses at earlier gestational ages. In addition, we have previously demonstrated the utility of assessing movement in fetuses with tachycardia [3] and bradycardia [2], who exhibit little or no FHR reactivity. In such cases it is critically important to have objective detection methods; however, the movement detection methods described here must be applied with caution because heart rate and rhythm changes can alter the QRS complex in the absence of movement, leading to overestimation of movement. Often these changes are more abrupt and transient than true movements and can be distinguished on that basis.

While the detectors perform as desired on real fMCG data, this should not be construed as a validation. True validation requires direct observation of movement, using ultrasound or some other surveillance technique. In the absence of ground truth, it is not possible to construct ROC curves to determine the detector thresholds. In addition, it is generally assumed that the amplitude of FHR acceleration reflects the vigor of fetal movement, but it may exhibit a complex relationship with the amplitude and velocity of fetal movement, as measured by our indices. With the recent development of techniques to perform simultaneous fMCG-ultrasound recording [9], it may be possible to perform such validation studies in the future.

In summary, actography is a highly useful adjunct of fMCG rhythm analysis. The methods described here are useful extensions of prior methods of fMCG actography.

Acknowledgments

This work was supported by the National Institutes of Health under Grant R01 HL63174.

References

1. Zhao H, Wakai RT. Simultaneity of foetal heart rate acceleration and foetal trunk movement determined by foetal magnetocardiogram actocardiography. *Phys Med Biol.* 2002; 47(5):839–846. [PubMed: 11931474]
2. Zhao H, Cuneo BF, Strasburger JF, Huhta JC, Gotteiner NL, Wakai RT. Electrophysiological characteristics of fetal atrioventricular block. *J Am Coll Cardiol.* 2008; 51(1):77–84. [PubMed: 18174041]
3. Wakai RT, Strasburger JF, Li Z, Deal BJ, Gotteiner NL. Magnetocardiographic rhythm patterns at initiation and termination of fetal supraventricular tachycardia. *Circulation.* 2003; 107(2):307–12. [PubMed: 12538433]
4. Popescu EA, Popescu M, Bennett TL, Lewine JD, Drake WB, Gustafson KM. Magnetographic assessment of fetal hiccups and their effect on fetal heart rhythm. *Physiol Meas.* 2007; 28(6):665–76. [PubMed: 17664620]

5. McCubbin JP, Murphy P, Eswaran H, Preissl H, Yee T, Robinson SE, et al. Validation of the flash-evoked response from fetal MEG. *Phys Med Biol.* 2007; 52(19):5803–5813. [PubMed: 17881801]
6. Nijhuis JG, Prechtl HF, Martin CB Jr, Bots RS. Are there behavioural states in the human fetus? *Early Hum Dev.* 1982; 6(2):177–195. [PubMed: 7094856]
7. Horigome H, Shiono J, Shigemitsu S, Asaka M, Matsui A, Kandori A, Miyashita T, Tsukada K. Detection of cardiac hypertrophy in the fetus by approximation of the current dipole using magnetocardiography. *Pediatric Research.* 2001; 50(2):242–245. [PubMed: 11477210]
8. Kay, S. *Fundamentals of Statistical Signal Processing: Detection Theory.* Vol. ch 5. Upper Saddle River, NJ: Prentice-Hall PTR; 1998.
9. Zhao H, Chen M, Van Veen BD, Strasburger JS, Wakai RT. Simultaneous Fetal Ultrasound/Doppler and Magnetocardiography. *IEEE Trans Biomed Eng.* 2007; 54(6):1167–71. [PubMed: 17549910]

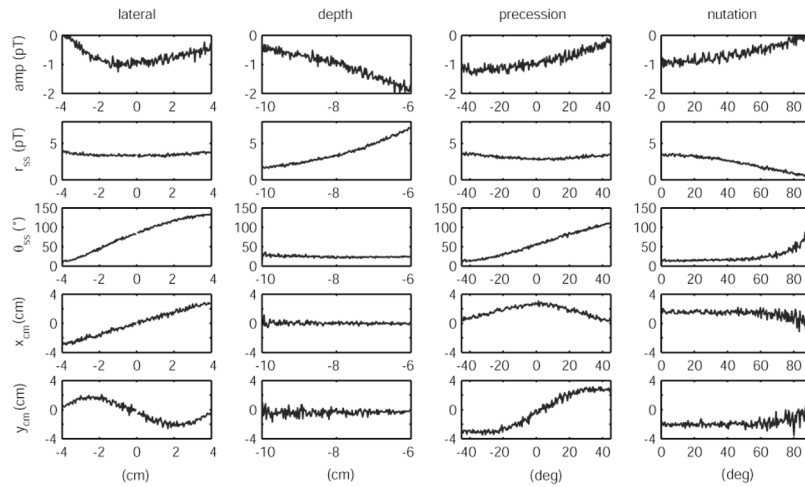


Fig. 1.

Simulated actograms comprised of the signal amplitude of the channel with largest signal (amp) and the indices r_{SS} , θ_{SS} , x_{CM} , and y_{CM} for four types of movement. Each graph contains 101 points, i.e. the variation step is equal to the x-axis range divided by 100.

Lateral: The source was 8 cm directly below the center channel of the sensor array, and the position was varied along the line $x=y$ from $x=-4$, $y=-4$ to $x=4$, $y=4$ cm at constant z , corresponding to a change primarily in lateral position. The dipole was pointing along the x -axis. For a dipole pointing along the y -axis, the graphs for x and y are transposed.

Depth: The source was directly below the center channel of the array ($x=y=0$), and the z position of the source was varied, corresponding to a change in source depth from 10 cm to 6 cm.

Precession: The position of the dipole was constant throughout the rotation. The dipole was located at approximate depth 8 cm, but was displaced laterally from the z -axis ($x=2$ cm, $y=2$ cm) because x and y vanish due to symmetry if the dipole is located exactly on the z -axis. The direction of the dipole was varied in the x - y plane from $x=0.707$, $y=-0.707$ to $x=0.707$, $y=0.707$, corresponding to a 90° rotation about the z -axis.

Nutation: The position of the dipole was constant throughout the rotation, and was the same as for precession. The direction of the dipole was initially pointing along the x -axis and then rotated to point along the z -axis, corresponding to a 90 degree rotation about the y -axis.

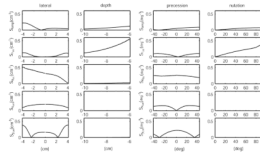
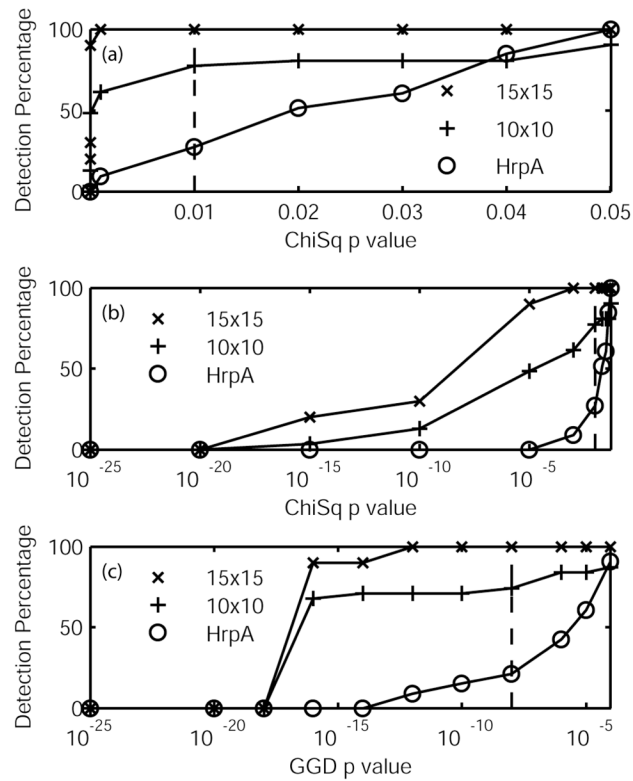


Fig. 2.

Graphs of normalized sensitivity, obtained by dividing the derivative of the corresponding graph in Fig. 1 by the rms fluctuation. The rms fluctuations were estimated from 10,000 independent simulations. This metric of detector performance facilitates comparison of the indices; e.g. the y-axis scale is the same for all graphs.

**Fig. 3.**

Detection percentages for movement associated with 15×15 (15bpm-15s), 10×10 (10bpm-10s) accelerations using statistics derived from all data, and with FHR-A (pattern A) using statistics derived from FHR-A data only. (a) Chi-square detections with p values plotted on linear scale; (b) Chi-square detections with p values plotted on log scale; (c) GGD detections. There were a total of 10 15×15 accelerations and 28 10×10 accelerations. Percentage of FHR-A detections based on maximum of GGD and Chi-Square detections (32). In contrast, there were no FHR-A detections when data statistics included transition or FHR-B data. Dashed lines indicate the preferred threshold values for the chi-square detector ($p=0.01$) and the GGD ($P_{Fp}= 10^{-8}$).

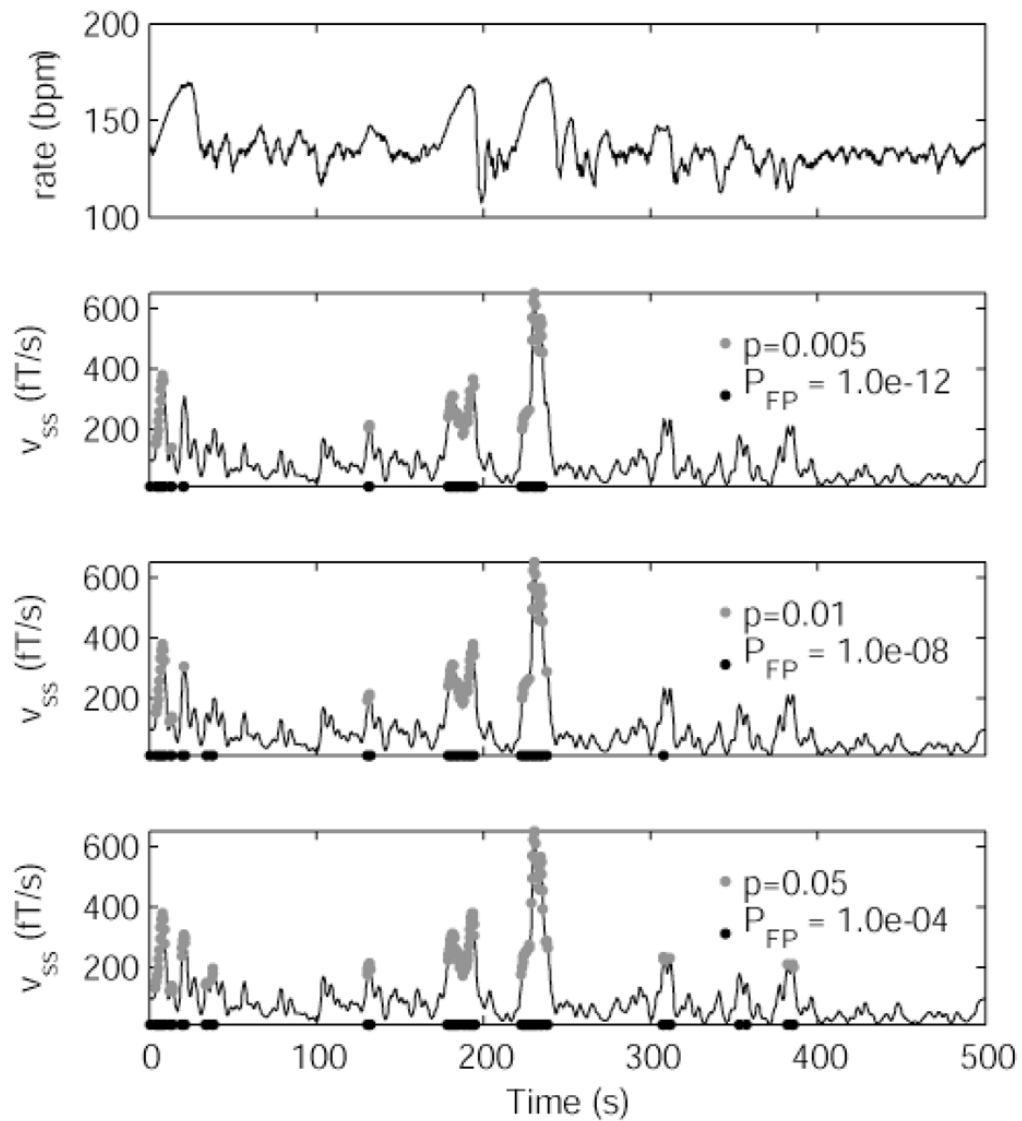


Fig. 4.

Detections for the chi-square detector (grey) and the GGD (black) for different values of p and P_{FP} , respectively. The detections are superimposed on actograms of v_{SS} . The corresponding FHR tracing is shown in the top panel, and depicts a transition from FHR pattern B to pattern A. The first half of the tracing, 0–250 s, is compatible with FHR pattern B, and shows three prominent FHR accelerations. This is followed by a period of transition, during which the tracing exhibits deviations from baseline that are substantial but are too small to be classified as accelerations. The FHR tracing is flat during the last 100 s, and is compatible with FHR pattern A, corresponding to fetal quiescence.

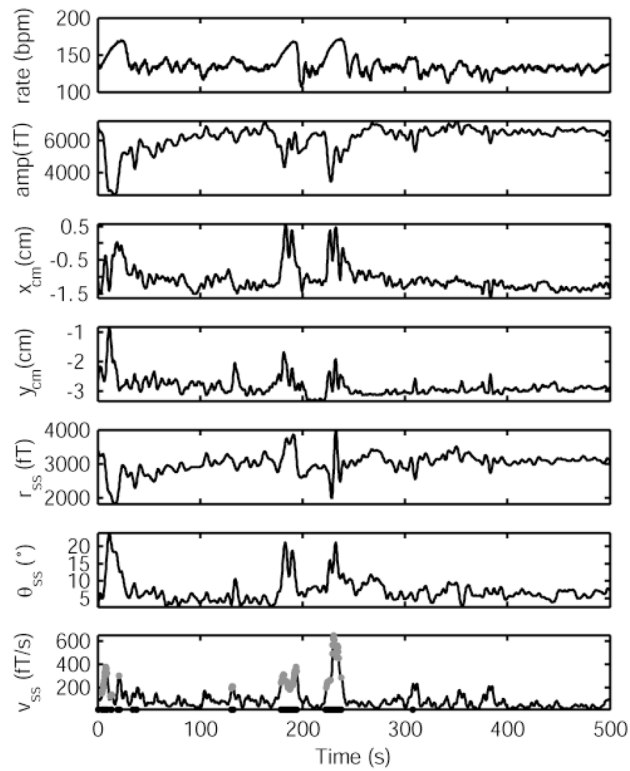


Fig. 5. Comparison of actograms from the same fetus as in Fig. 4. The top panel shows the FHR tracing; below are actograms derived from the signal amplitude of the channel with largest signal (amp) and the indices x_{CM} , y_{CM} , r_{SS} , θ_{SS} , and v_{SS} . Superimposed on the v_{SS} actogram are detections for the chi-square detector ($p=0.01$) in grey and the GGD ($P_{FP}=10^{-8}$) in black.

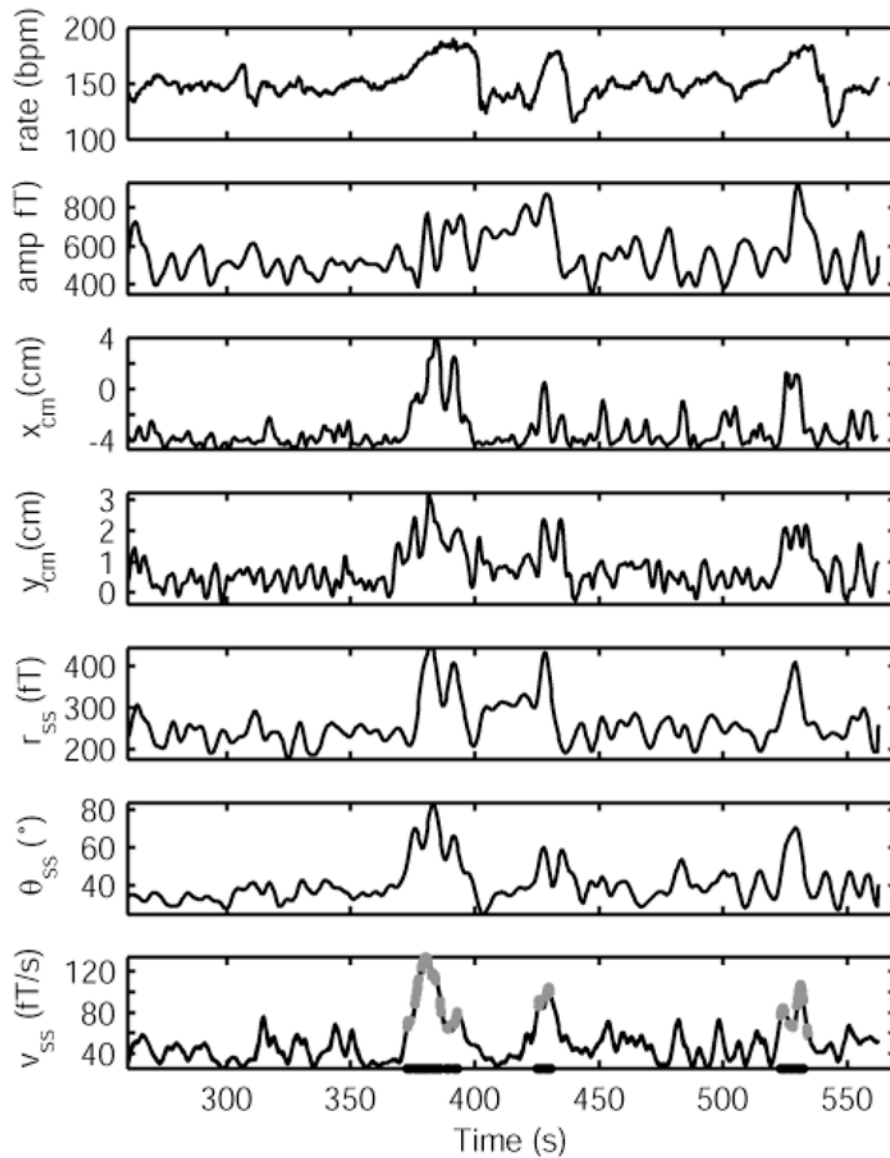


Fig. 6. Comparison of actograms from a full-term neonate at conceptional age 48 weeks. The top panel shows the heart rate tracing; below are actograms derived from the signal amplitude of the channel with largest signal (amp) and the indices x_{CM} , y_{CM} , r_{SS} , θ_{SS} , and v_{SS} .

Table 1

Number of Gaussian Channels (prior to SVD) and number of SVD components of $\Delta\mathbf{X}/\Delta t$ during fetal heart rate pattern A (FHR-A), pattern B (FHR-B), and transition from pattern A to pattern B based on Lilliefors test at significance levels of 1, 3, and 5%. FHR-B data contained all 15 bpm-15 s and some 10 bpm-10 s accelerations. FHR-A data was quiescent with no 5 bpm-5 s accelerations. The transition data comprised the remainder of the evaluated data.

FHR pattern	Significance level	Gaussian Channels	Gaussian SVD Components
A	0.01	(263/333) 79%	(63/83) 75.9%
A	0.03	(225/333) 67.6%	(57/83) 68.7%
A	0.05	(206/333) 61.9%	(52/83) 62.6%
Transition	0.01	(143/444) 32.2%	(21/45) 46.7%
Transition	0.03	(118/444) 26.6%	(19/45) 42.2%
Transition	0.05	(103/444) 23.2%	(18/45) 40.0%
B	0.01	(25/296) 8.4%	(10/43) 23.3%
B	0.03	(22/296) 7.4%	(9/43) 20.9%
B	0.05	(18/296) 6.1%	(8/43) 18.6%